CRYSTAL GROWTH & DESIGN

pubs.acs.org/crystal

Article

Tailor-Made Nanoseeds for the Synthesis of Zeolites with Nanosized Dimensions

Published as part of a Crystal Growth and Design virtual special issue on Zeolite Crystal Engineering

Zihao Wang, Tongtong Meng, Jiani Xu, Yanfeng Shen, Yida Zhou, Yuhan Liu, Dong Fan, Xinmei Liu, Shutao Xu,* and Zhengxing Qin*

Cite This: *Cryst. Growth Des.* 2023, 23, 6450−6460

Read Online

ACCESS | Metrics & More | Article Recommendations | Supporting Information

ABSTRACT: While seeding is a long-established strategy for the synthesis of zeolites with the desired phase in a faster crystallization rate and it is believed that the added seeds are at least partially dissolved in the synthetic gel for zeolite nucleation and growth, the solubility of seed crystals is seldom explored as a potential modulating factor for the tuning of zeolite properties. Herein, NH_4F etching was used as a "chemical scissors" for the cutting of existing zeolites into nanosized crystals with enhanced solubility for the subsequent synthesis pursuing for zeolites with nanosized dimensions. Exemplified by the synthesis of mordenite, the tailor-made seeds reduced the size of the synthetic products by 1.9 times and further by 8.5 times compared with the synthesis seeded by the uncut sample and without seeding, respectively. Further, the general applicability of the size tailoring strategy is illustrated by the synthesis of ZSM-5 nanosheets using the top-down prepared nanoseeds. Considering the tunability and convenience of NH_4F etching in the postsynthesis engineering of zeolite particle size, it is envisaged that the successful utilization of this chemical cutting strategy will be instrumental in many systems aiming for nanosized zeolite synthesis.

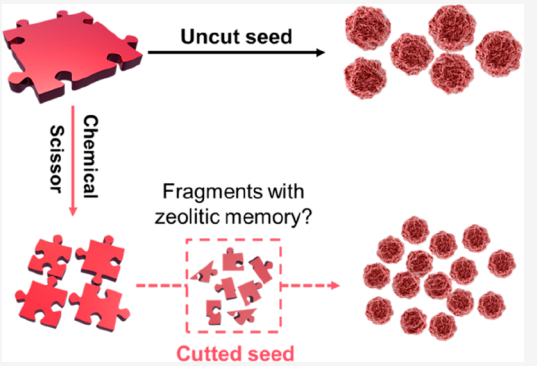

INTRODUCTION

Zeolites are microporous crystalline aluminosilicates that are widely utilized in catalysis, adsorption, separation, pollution control, and many new and cutting-edge technologies,[1−6] thanks to their outstanding stability, unique shape selectivity, and tunable physicochemical properties including, but not limited to, ion-exchange capacity, acidity properties, framework compositions, and hydrophilicity/hydrophobicity. In many of the applications, the reduction of zeolite particle size to a nanometric dimension plays an important role for the upgrading of their physical and chemical properties. Because of their larger active external surface area and shorter diffusion distance, nanosized zeolites (or zeolite domains with nanosized dimensions) are widely used particularly in the fields of catalysis and adsorption applications.[7,8] The accompanying favorable outcomes include high catalytic activity, improved products selectivity, greater resistance to coke formation, etc.[9,10]

Motivated by the desire for zeolites with improved sorption or catalytic performance, there are several approaches available for the synthesis of zeolites that have one or more dimensions on the order of 100 nm or less. Some classic examples include the synthesis of colloidal zeolites from clear solutions,[11−14] the design of finned zeolites with nanosized protrusions,[15] the preparation of two-dimensional or layered materials through surfactant templated synthesis,[16−19] or the top-down synthesis through the assembly−disassembly−organization−reassembly (ADOR) strategy.[20,21] Besides the tailored design of nanozeolite products with uniform size and dimension, the preparation of hierarchical zeolites is another way for the preparation of zeolite crystals with nanosized microporous domains.[22,23] While there is no clear boundary between mesoporous materials and some of the pillared zeolites composed of nanosheets, many of the samples with a hierarchical porosity is made of nanosized zeolite domains of a broad particle size distribution and nonuniform crystal morphology, especially for those prepared by postsynthesis modifications[24,25]

Different from the preparation of hierarchical or nanosized zeolites that with a straightforward goal to provide zeolite crystals with ultrasmall dimensions to improve the mass transport efficiency, seeding as a multiple-purpose method has also been widely applied in zeolite synthesis.[26,27] It can be used

Received: April 7, 2023
Revised: July 14, 2023
Published: July 26, 2023

https://doi.org/10.1021/acs.cgd.3c00427
Cryst. Growth Des. 2023, 23, 6450−6460

to accelerate the crystallization process and increase the crystal purity. It is the core part of an environmentally friendly and low-cost route for reducing or even eliminating the use of organic structure-directing agents.[28] In addition, seeding also offers an alternative to the templated ones for the synthesis of zeolite nanocrystals.[29−31] In this respect, perhaps the most popular type of seeds is the variety of silicalite-1 zeolites synthesized in the presence of TPA^+ and OH^-.[31] Regarding the crystallization mechanism in seeded synthesis, the group of Xiao proposed a core−shell growth mechanism in the seed-directed synthesis of zeolite Beta.[32] In that case, although a partial dissolution of the added seeds was speculated, the remaining undissolved seeds act as the core for the epitaxial growth of the Beta zeolite. Alternatively, the group of Sano suggested that, in the study of interzeolite conversion, the dissolution of FAU zeolite in TEAOH solution provided aluminosilicate fragments with local orders that assemble and evolve into beta zeolite.[33]

While there is a consensus that the added seeds will dissolve at least partially in the new synthesis medium, and there is evidence showing that the dissolved debris carry a memory of the parent sample that facilitates the nucleation of the daughter,[26,27,34] the solubility of zeolite crystals is seldom explored as a potential modulating factor for the tuning of zeolite properties. In practice, it is often the products of the former synthesis that are used directly for the seed-assisted synthesis of daughter zeolites with the same framework. The solubility of such crystals in a zeolite synthesis gel cannot be high as they are already resistant to the high pH of the mother liquor of the previous synthesis. In the present work, the combined oxalic acid leaching and NH_4F etching or the fluoride etching alone was used as a "chemical scissors" for the tailoring of nanosized zeolite crystals, which will be used as seeds in the subsequent synthesis. It is envisaged that the top-down prepared seeds with a substantially decreased particle size and an introduced mesoporosity, hence an enhanced solubility, will work as a sacrificial seed that is favorable for the synthesis of zeolite with nano sized dimension. As a proof of concept, the synthesis of mordenite zeolite was used as demonstration purpose, both because of it significant industrial relevance,[35,36] and because of the established experience in the postsynthesis engineering of this zeolite.[37]

2. EXPERIMENTAL SECTION

2.1. Chemicals and Materials Used in the Present Study. Sodium hydroxide (NaOH, 99.0 wt %), tetraethyl orthosilicate (TEOS, 99%), sodium aluminate ($NaAlO_2$), ammonium fluoride (NH_4F), ammonium sulfate ($(NH_4)_2SO_4$), oxalic acid dihydrate, aluminum sulfate octadecahydrate ($Al_2(SO_4)_3{\cdot}18H_2O$), and tetrapropyl ammonium bromide (TPABr), all in the Analytical Reagent grade, were purchased from the Sinopharm Chemical Reagent Co., Ltd. Silica sol (30.0 wt %) was purchased from Qingdao Haiyang Chemical Co., Ltd. All chemicals were used directly without further purification. The commercial mordenite zeolite (denoted MOR-P) used in this study was purchased from Zeolyst. The Si/Al ratio of this sample determined by XRF is 6.8. The commercial MFI-90 zeolite used in this study was supplied by Clariant.

2.2. Nanohierarchical Mordenite (MOR) Zeolite Engineered by Sequential Oxalic Acid Leaching and NH_4F Etching. The following are the procedures for the preparation of MOR zeolite crystals with a nanosized dimension. First, 80 g of $(NH_4)_2SO_4$ was dissolved in 800 g of deionized water, and 80 g of the commercial MOR zeolite was dispersed in the $(NH_4)_2SO_4$ aqueous solution. The ammonium exchange was carried out at 90 °C for 3 h under stirring (480 rpm) in an oil bath. The same ion-exchange was repeated three times with intermediate vacuum filtration and washing. After the third ion-exchange, the sample were collected by vacuum filtration, washed thoroughly using deionized water, and dried in an oven at 100 °C for more than 12 h. Then, 63 g of oxalic acid dihydrate was dissolved in 687 g of deionized water to obtain an 8 wt % oxalic acid solution, to which was added 36 g of the NH_4-exchanged MOR zeolite. The oxalic acid treatment was carried out at 90 °C for 46 h under continuous stirring (480 rpm). After that, the sample was vacuum filtrated, washed thoroughly using deionized water until the pH was close to neutral. The collected sample was dried in an oven at 100 °C overnight. Finally, NH_4F etching of the MOR zeolite was carried out. For this purpose, 300 g of ammonium fluoride solution with a concentration of 30 wt % was prepared first, then 10 g of the oxalic acid treated MOR sample was added. The NH_4F etching was carried out at 50 °C for 30 min under the combination of mechanical stirring and ultrasonic agitation. Then the sample was vacuum filtrated, washed, and dried in an oven at 100 °C overnight. This sample was denoted MOR-F.

2.3. Hydrothermal Synthesis of MOR Zeolites in the Absence and Presence of Seeds. The following are the procedures for the synthesis of MOR zeolite samples. First, NaOH was dissolved in a certain amount of deionized water, and then $NaAlO_2$ was added while stirring at room temperature. The mixture was homogenized for 30 min to get a clear solution. After that, silica sol was added dropwise. Then 30 min after the last drop of silica, either MOR-P or MOR-F, both in their NH_4-form, was added in the case of the seed-assisted synthesis. The added amount was 10 wt % based on silica. The obtained whitish gel was continuedly stirred at room temperature overnight. The final precursor mixture was transferred into a Teflon-lined stainless autoclave. The hydrothermal synthesis was carried out at 170 °C for 48 h. The obtained products were filtrated, washed with deionized water until the pH of the last washing solution was less than 8. The washed solid was put into an oven and dried overnight at 100 °C for 12 h to obtain the Na-form mordenite zeolites. In the present work, two groups of mordenite zeolite samples were synthesized by changing the H_2O/SiO_2 of the aluminosilicate gels. The detailed gel compositions for the synthesis of mordenite zeolites are collected in Table 1.

Table 1. Compositions of the Gels for the Synthesis of Mordenite Zeolites

Group	Sample	SiO_2	Al_2O_3	Na_2O	H_2O	Seed
I	MOR-1	1.0	0.079	0.23	15.0	-[a]
	MOR-1S	1.0	0.079	0.23	15.0	MOR-P
	MOR-1SF	1.0	0.079	0.23	15.0	MOR-F
II	MOR-2	1.0	0.079	0.23	38.0	-[a]
	MOR-2S	1.0	0.079	0.23	38.0	MOR-P
	MOR-2SF	1.0	0.079	0.23	38.0	MOR-F

[a]No seeds were added during the synthesis.

2.4. Hydrothermal Synthesis of ZSM-5 Zeolites with or without the Tailor-Made Seeds. First, the seeds for the synthesis of ZSM-5 zeolites were prepared by fluoride etching, the chemical Scissors, using the following procedure: 5 g of the pristine MFI-90 zeolite was dispersed in 100 g of 40 wt % NH_4F aqueous solution and react at 50 °C for up to 30 min under mechanical stirring and ultrasonication. The etched products were thoroughly washed with distilled water after the fluoride medium treatment and dried in an oven at 100 °C overnight. The sample was denoted MFI-90-F.

The following are the procedures for the synthesis of ZSM-5 zeolite samples. First, $Al_2(SO_4)_3{\cdot}18H_2O$ was dissolved in a certain amount of deionized water, and then TPABr was added while stirring at room temperature. The mixture was homogenized for 30 min to get a clear solution. After that, TEOS was added dropwise. The obtained whitish gel was continuously stirred at room temperature overnight. Then, seed and NH_4F were added sequentially while stirring at room temperature for 2 h under continuous stirring (600 rpm). The parent MFI-90 and MFI-90-F were used as seeds (10 wt.% based on silica)

https://doi.org/10.1021/acs.cgd.3c00427
Cryst. Growth Des. 2023, 23, 6450−6460

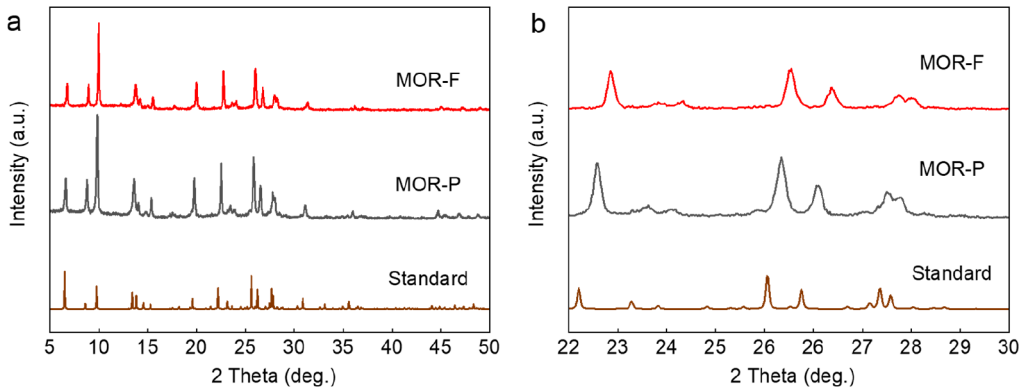

Figure 1. XRD patterns of the MOR-P and MOR-F zeolites in wide (a) and narrow (b) two Theta degree ranges.

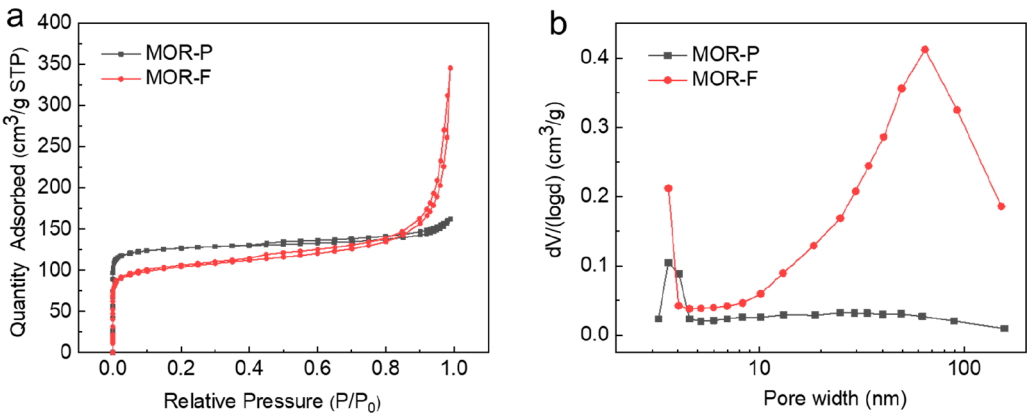

Figure 2. Ar adsorption−desorption isotherms (a) and pore size distribution (b) of the MOR-P and MOR-F zeolites.

for comparison purposes. The composition of the final gel is 0.033 $Al_2(SO_4)_3$·18 H_2O: 1.0 TEOS: 0.13 TPABr: 0.56 NH_4F: 23.13 H_2O. The precursor mixture was transferred into a Teflon-lined stainless autoclave and hydrothermally treated at 150 °C for 24 h. The obtain products were filtrated, washed with deionized water until the pH of the last washing solution was less than 8. The washed solid was put into an oven and dried overnight at 100 °C for 12 h to obtain the ZSM-5 zeolites.

2.5. Characterization. The phase purity of the prepared zeolite samples was checked by Bruker D8 Advanced X-ray Diffraction (XRD). The morphology and size of the mordenite zeolites were characterized by using a low-voltage-high-resolution field emission scanning electron microscope (SEM, JSM-7900F, JEOL). The size and interstitial mesoporosity were checked by a JEM-2100 Transmission Electron Microscope produced by JEOL. An inductively coupled plasma optical emission spectrometer (ICP-OES) was used for the determination of the Si/Al ratio. Autosorb iQ3 (Qutant chrorome) was used to measure the porosity properties of zeolites with N_2 (77 K) or Ar (87 K) as the probe molecule. The Brunauer−Emmett−Teller (BET) and *t*-plot methods were used to calculate the specific surface area and micropore volume of the zeolite samples. Fourier transform infrared spectra (FTIR) analysis were recorded on Bruker Tensor 27 instrument with a mercury cadmium telluride detector. The samples (20 mg) were pressed into a self-supporting wafer and placed into a quartz cell. Subsequently, the samples were pretreated at 420 °C for 5 h under vacuum. After pretreatment, the samples were cooled to room temperature for the recording of the spectra from 4000 to 1000 cm^{-1}. The spectrum was obtained by averaging 32 scans at a resolution of 4 cm^{-1}. Solid-state NMR spectra were recorded on a Bruker Avance III 500 MHz spectrometer. ^1H MAS NMR spectra were collected at 500.13 MHz with a 3.2 mm HXY probe with a recycle delay of 10 s and a spinning speed of 20 kHz. The chemical shifts were referenced to adamantane at 1.74 ppm. Before the ^1H MAS NMR measurements, the samples were dehydrated at 420 °C under a vacuum below10^{-3} Pa for 12 h. ^{27}Al MAS NMR spectra were collected at 156.4 MHz with a spinning speed of 12 kHz, and the chemical shifts were referenced to 1 mol/L Al $(NO_3)_3$ solution at 0 ppm. ^{29}Si MAS NMR spectra were collected at 119.2 MHz with a spinning speed of 12 kHz, and the chemical shifts were referenced to kaolin at −91.5 ppm.

2.6. Catalytic Performance. Before the catalytic test, the mordenite zeolite samples were ion-exchanged to the NH_4-form as described above. In order to get the H-form for catalysis, the NH_4-exchanged samples were calcined in a muffle furnace at 550 °C for 5 h with a heating ramp of 1 °C/min. Dimethyl ether (DME) carbonylation reactions were performed in a fixed-bed reactor, and 0.3 g of the catalyst (40−60 mesh) was loaded into the reactor and pretreated (heating rate 1 °C/min) in Ar (30 mL/min) at 400 °C for 2 h. Afterward, the temperature was reduced to 200 °C, and a reactant gas mixture (DME/CO/N_2 = 5:35:60) was introduced with a gas hourly space velocity (GHSV) of 1800 mL/(g·h). The reaction pressure was 2.0 MPa. The products were analyzed online by a gas chromatograph (Agilent 7890B) equipped with a TCD and a flame ionization detector (FID) using a TDX-1 packed column and a PoraPLOT Q capillary column, respectively.

3. RESULTS AND DISCUSSION

3.1. Nanohierarchical Mordenite Seeds Tailored by Sequential Oxalic Acid Leaching and NH_4F Etching. In the present work, the tailoring of the particle size of the mordenite zeolite seeds was conducted through sequential oxalic acid leaching and NH_4F etching. The oxalic acid treatment was carried out for the introduction of framework interruption points in the form of hydroxyl nests left by dealumination.[37] Different from the previous study, the concentration of the NH_4F solution was decreased by 10 wt.

https://doi.org/10.1021/acs.cgd.3c00427
Cryst. Growth Des. 2023, 23, 6450−6460

% to mitigate the hydrolysis of NH_4F,[38] so as to slow down the etching kinetics and to get a better control over the fluoride etching process.

The XRD patterns of the parent mordenite zeolite sample, MOR-P, and the NH_4F treated counterpart, MOR-F, are shown in Figure 1a. MOR-P is a phase pure microporous mordenite sample with a high crystallinity[37] and a limited mesoporosity (Figure 2 and Table 2).[39] After NH_4F etching, there is an obvious decrease in the intensity of XRD peaks. In accordance with the crystallinity degradation, a nearly 30% reduce of micropore volume was measured by Ar physisorption analysis (Figure 2 and Table 2).[39] On the other side, the applied NH_4F etching turned the microporous mordenite into a highly mesoporous sample. This hierarchical characteristic is reflected by the substantially increased sorption capacity for Ar in a relative pressure range higher than 0.8 in the case of MOR-F (Figure 2). The mesopore volume of this sample is 0.33 cm^3/g, which is more than 6 times higher than that of the MOR-P sample. Accompanying these changes, the Si/Al ratio of the mordenite sample increased sharply from 6.8 to 21.0 after sequential oxalic acid leaching and fluoride etching. In accordance with this increase, the XRD peak positions shift rightward in the case of the MOR-F sample (Figure 1b).

Table 2. Collection of Porosity and Si/Al Ratio Data of the Mordenite Samples

Sample	S_{BET}[a] (cm^2/g)	V_{Mic}[b] (cm^3/g)	V_{Mes}[c] (cm^3/g)	Si/Al[d]	Si/Al[e]
MOR-P	443	0.15	0.05	6.8	6.8
MOR-F	345	0.11	0.33	21.0	28.1
MOR-1	346	0.13	0.01	4.1	4.3
MOR-1S	418	0.16	0.03	4.6	4.7
MOR-1SF	455	0.17	0.03	4.8	4.8
MOR-2	387	0.14	0.04	5.1	5.1
MOR-2S	413	0.15	0.08	5.4	5.5
MOR-2SF	432	0.16	0.10	5.5	5.6

[a]Specific surface area calculated by BET method. [b]Micropore volume calculated with t-plot method. [c]Mesopore volume = Total volume − Micropore volume. [d]Si/Al measured by ICP. [e]Si/Al calculated from ^{29}Si MAS NMR.

Apparently, the applied NH_4F etching imposed a big impact on the mordenite zeolite crystals. This is further confirmed from a microcosmic point of view. As expected, the particle size of the zeolite crystals decreased substantially after the applied NH_4F etching. As the observation of the MOR-F sample by SEM shows clearly, the originally plate-shaped crystals (Figure 3a,b) were substantially segmented by the NH_4F treatment. This is in line with our previous studies.[37,40] A statistic result of the particle size distribution based on the measurement of more than 50 individual zeolite crystals is shown in Figure S1. It shows that the particle size of the MOR-F sample is centered around 100 nm (Figure S1b). In the case of MOR-P, the particle size distribution is broader and the peak maximum is two times higher than that of MOR-F (Figure S1a). The characterization of MOR-P and MOR-F by TEM confirmed the disassembly of the intergrown crystals (Figure 3c,d). In addition, it confirmed the presence of a substantial inter- and intraparticle mesoporosity in the segmented crystals (Figure 3 and Table 2).

Herein, the set of data reported above show consistently that with the combined oxalic acid etching and NH_4F etching, it is able to transform an existing zeolite sample of an aggregated nature and a broad particle size distribution into a hierarchical zeolite with a substantially increased Si/Al ratio as well as small and uniform crystal size. It has been reported that a mordenite zeolite with a higher Si/Al ratio is more soluble in an alkaline medium.[41,42] Therefore, we envisaged that the tailor-made zeolite with integrated high Si content, large mesopore volume, and small crystal size will serve as a good seed for the boosting of zeolite nucleation and crystallization.

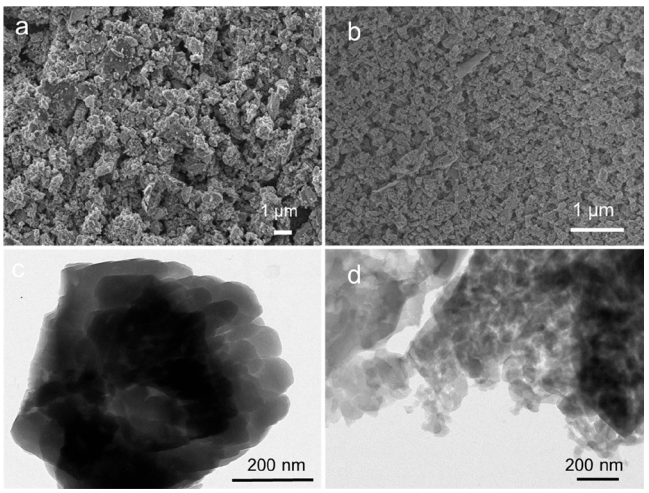

Figure 3. SEM (a, b) and TEM (c, d) images of the MOR-P (a, c) and MOR-F zeolites (b, d).

3.2. Mordenite Zeolite Samples Prepared in the Absence and Presence of Seeds. *3.2.1. Seeded Synthesis of Mordenite Zeolites: The Impact of Different Seeds.* The synthesis was carried out first using the gel composition classified as Group I (Table 1). Three mordenite zeolite samples were prepared following the same recipe, either in the absence of seeds (MOR-1), or in the presence of the MOR-P (MOR-1S) and MOR-F (MOR-1SF) zeolites. The XRD patterns for the obtained zeolite crystals are listed in Figure 4. Taking the crystallinity of the MOR-1 sample as 100%, the relative crystallinity of MOR-1S and MOR-1SF were calculated using (200), (330), (150), (202), and (350) reflections by

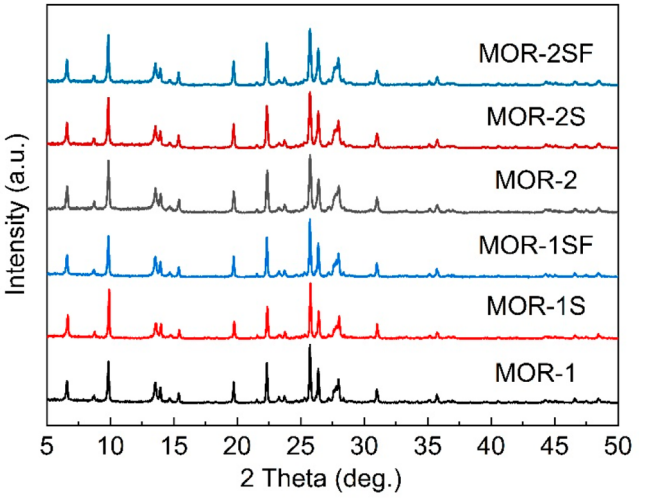

Figure 4. XRD patterns of the two groups of MOR samples synthesized in the present study.

https://doi.org/10.1021/acs.cgd.3c00427
Cryst. Growth Des. 2023, 23, 6450−6460

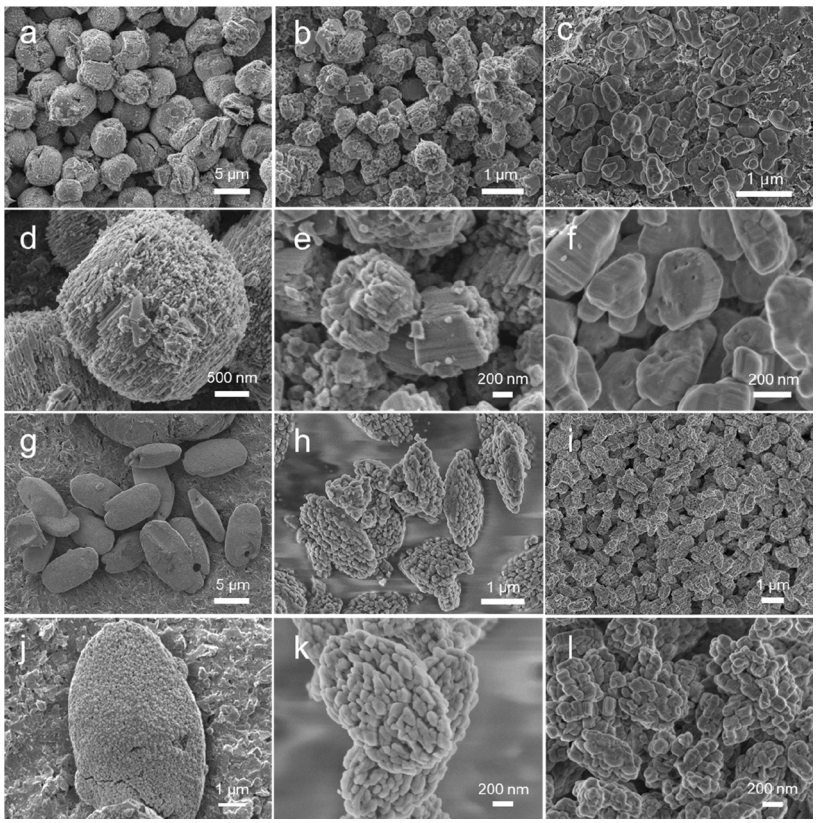

Figure 5. SEM images of the MOR samples: MOR-1 (a, d); MOR-1S (b, e); MOR-1SF (c, f); MOR-2 (g, j); MOR-2S (h, k); MOR-2SF (i, l)

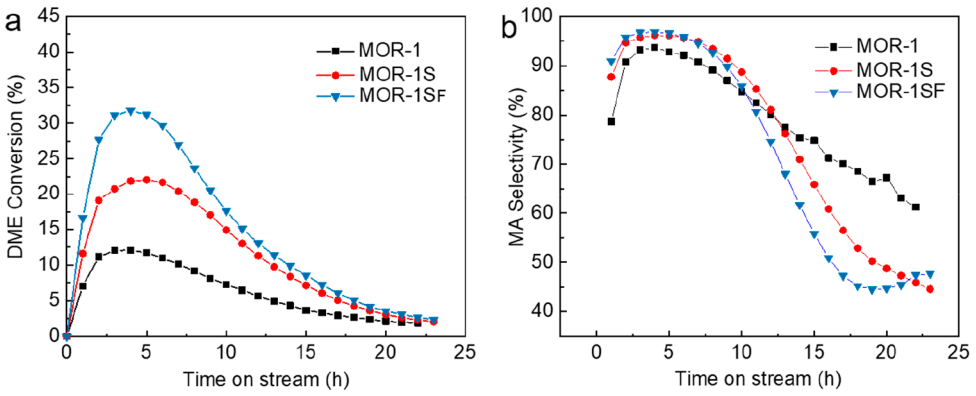

Figure 6. DME carbonylation over group I mordenite zeolite samples: The change of the DME conversion rate (a) and methyl acetate selectivity (b) over time on stream.

adding their peak areas and compared with that of the MOR-1 sample.[43] The relative crystallinity of MOR-1S and MOR-1SF calculated in this way are 102% and 106%, respectively, indicating that the addition of seeds is favorable for the crystallization of mordenite zeolite. The porosity properties of these samples in the Na-form were evaluated using N_2 as the probe molecule. All the three isotherms show a typical microporous sorption characteristic throughout the whole relative pressure (P/P_0) range (Figure S2), indicating that these samples are purely microporous.[39] The micropore volumes of MOR-1S and MOR-1SF are higher than that of the MOR-1 sample (Table 2). The adsorption and desorption branches of the isotherms are not closed, even in the P/P_0 range lower than 0.45 (Figure S2). This is because the presence of Na^+ cations in the 1D channel hampered the desorption of the N_2 molecules.

The SEM images of the Group I zeolite samples are shown in Figure 5a-f. The MOR-1 sample is presented as a spherical granular morphology with a particle size of 3−5 μm (Figure 5a, d and Figure S3a). The outermost layer of the crystals is covered by needle-shaped nanocrystals. Such a morphology is typical for mordenite zeolites with a low Si/Al ratio.[41,44] Indeed, the Si/Al ratio of the MOR-1 sample determined by ICP and ^{29}Si MAS NMR methods is 4.1 and 4.3, respectively (Table 2). The morphology of the MOR-1S sample remains granular (Figure 5b, e), but the morphology is closer to that of cylindrical bundles. The particle size of this sample is distributed in the 0.6−1.2 μm range (Figure S3b). Apparently, the presence of seeds, even if it is a commercial zeolite with a

https://doi.org/10.1021/acs.cgd.3c00427
Cryst. Growth Des. 2023, 23, 6450−6460

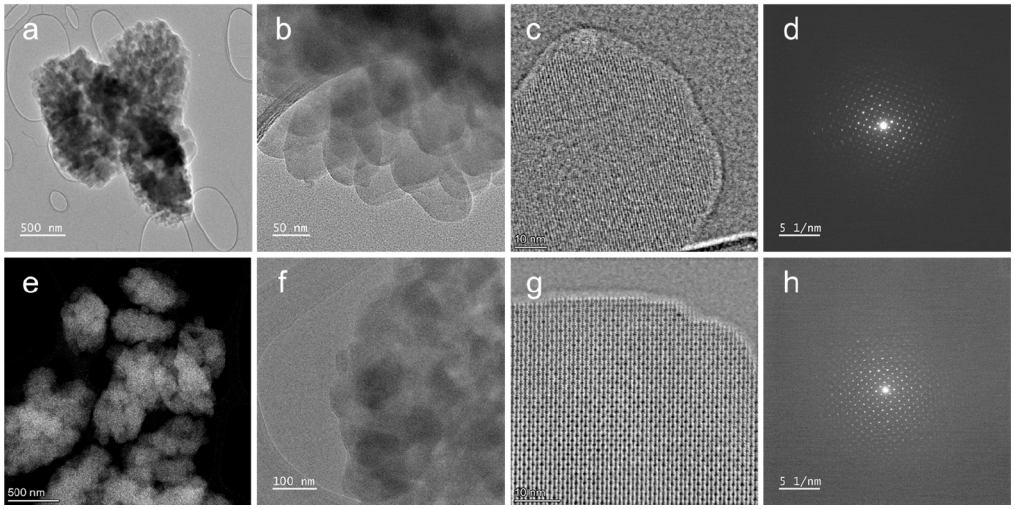

Figure 7. TEM images and single crystal diffraction patterns of MOR-2S (a-d) and MOR-2SF (e-h).

broad pore size distribution, sharply decreased the size of the mordenite crystals. On the other hand, the Si/Al ratio of the MOR-1S sample determined by ICP method is 4.6 (4.7 by ^{29}Si MAS NMR method, Table 2), which is 0.5 higher than that of MOR-1. In the case of the MOR-1SF sample, the morphology turns into a single grain structure with an obviously smoother crystal surface (Figure 5c, f). The sample is homogeneous in crystal size, with a particle size distribution between 400 and 600 nm (Figure S3c), which is 2−3 times smaller than the size of MOR-1S, pointing to the fact that smaller seeds lead to smaller zeolite products. On the other hand, the Si/Al ratio of the synthesized product increases further to 4.8 as determined by both ICP and ^{29}Si MAS NMR methods.[43]

3.2.2. DEM Carbonylation over Mordenite Zeolites: The Impact of Particle Size. Several recent studies showed that zeolites with hierarchical porosity or nanosized dimensions improved the catalytic performance in DME carbonylation thanks to the enhanced mass transfer.[45−49] In the present work, the impact of the particle size on the DME reaction performance was tested using the Group I zeolites demonstrated above. The preliminary catalytic results confirmed that decreasing the particle size of zeolite crystals has a positive impact on the DME carbonylation reaction. This can be seen clearly from the data shown in Figure 6. While all the tested samples show a similar trend in the change of conversion rate (Figure 6a), with the sequential increase and decrease corresponding to the induction period and gradual deactivation, the highest DME conversion over MOR-1 is 12% under the applied catalytic conditions. On the other side, the highest DME conversion rates of MOR-1S and MOR-1SF increased to 22% and 32%, respectively.[50,51] Meanwhile, the smaller crystals also show a relatively higher selectivity to methyl acetate during the active range (Figure 6b).

3.2.3. Impact of Synthesis Conditions: H_2O/SiO_2 Ratio as a Case Study. The catalytic results reported above show clearly a positive impact of reducing the crystal size on zeolite performance. In fact, many synthetic parameters, including, but not limited to, synthesis temperature, the amount of seeds, the aging of the synthetic precursors, are favorable for the synthesis of zeolites with nanosized dimensions.[11−13,52,53] While it is beyond the scope of the present study to optimize these synthetic conditions, we will use this space to shed light on the beneficial impact of routine operation variables on the size and morphology of zeolites during the seed assisted synthesis. Herein, by increasing the H_2O/SiO_2 ratio of the synthesis gel from 15 to 38, and keep other molar ratio unchanged, another three mordenite zeolites were prepared, again, in the absence or in the presence of commercial or homemade zeolite seeds (Table 1). For comparison, these samples are classified into group II as a category.

Increasing the amount of H_2O resulted in a decline in the alkalinity and concentration of the gel. This results in a general increase in the Si/Al ratio of the synthesized products (Table 2), without impacting the apparent crystallinity of the synthesized products. The peak intensities of the group II samples are comparable to that of the group I zeolites (Figure 4). Taking the same method for the calculation of relative crystallinity, by assuming the crystallinity of the reference sample MOR-2 as 100%, the calculated relative crystallinity of samples MOR-2S and MOR-2SF are 100% and 102%, respectively. On the other side, the size and morphology of the group II zeolite crystals change substantially in comparison to the group I zeolites. As revealed by SEM observation, while the MOR-1 zeolite is presented as spherical granules, the MOR-2 sample has a plate-like morphology with a much larger size in the elongated dimension (Figure 5g, j). The statistical calculation of the particle size along this dimension results in a distribution between 7.8 and 9.2 μm (Figure S3d). The MOR-2S sample keeps the plate-like morphology, but with a noticeable decrease in crystal size (Figure 5h, k). One can notice that the size and morphology of the MOR-2S sample resemble that of MOR-P that serves as the seeds for its synthesis. A statistical analysis of the particle size along the longest dimension gives a distribution that varies from 1.6 to 2.3 μm (Figure S3e). In the case of MOR-2SF, the morphology of the zeolite particles is ill-defined (Figure 5i, l). The particle sizes of the assembled crystals varies between 0.5 and 1.5 μm (Figure S3f). The tiny particles that make up the assembly are irregularly shaped, which have a size range of 80 to 180 nm.

The size and interstitial structure properties of the MOR-2S and MOR-2SF zeolites were studied further by TEM and N_2 physisorption. The characterization results confirm that, on the one hand, MOR-2SF has a smaller particle size than MOR-2S (Figure 7a, e); on the other hand, both MOR-2S and MOR-2SF have an interstitial mesoporosity as a result of the

https://doi.org/10.1021/acs.cgd.3c00427
Cryst. Growth Des. 2023, 23, 6450−6460

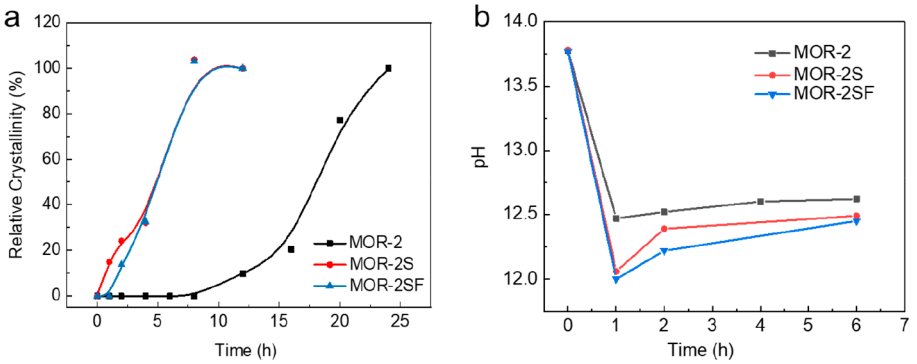

Figure 8. Zeolite growth kinetics curves and the evolution of pH value in the early stage of crystallization during the synthesis of the group II MOR samples.

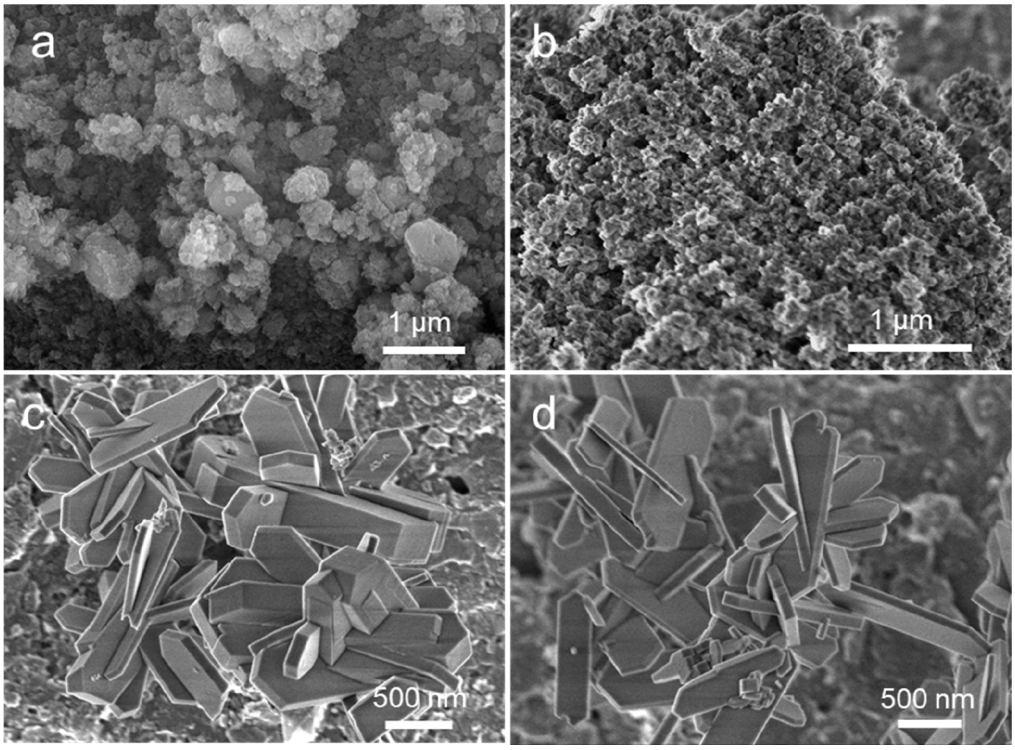

Figure 9. SEM images of the MFI-90 (a), MFI-90-F (b), ZSM-5-1 (c), and ZSM-5-2 (d) zeolite samples.

assembly of the intergrown nanocrystals of high crystallinity (Figure 7). These two points are further illustrated by the N_2 physisorption results. Namely, the three samples have a microporosity that is comparable to that of the high quality MOR-P sample (Table 2), pointing to the high crystallinity of the group II samples. On the other hand, these zeolites show a different adsorption behavior in the high P/P_0 range. As can be seen from Figure S2c, the isotherms of MOR-2 remain largely microporous, with a limited uptake of N_2 molecules in the P/P_0 range higher than 0.8. In the case of MOR-2S, the uptake of N_2 molecules in the 0.8−1.0 P/P_0 range increases sharply and the amount of N_2 adsorbed in the case of MOR-2SF increases further, as a result of the presence of substantial sorption capacity contributed by the interstitial porosity between nanoparticles (Figure 7).

3.2.4. Role of the Tailor-Made Seeds: A Perspective Based on the XRD and pH Measurement. In order to study the impact of seeds on the synthesis kinetics, the crystallization process of the group II samples was tracked. The same batch of aluminosilicate gel was prepared and divided equally into several parts for independent crystallization. Intermediate samples were collected, the samples were washed thoroughly and dried, and the XRD patterns measured. It can be seen from Figures S4−S6 that, in the absence of seeds, the synthesis of MOR-2 passed more than 12 h an induction period before the occurrence of the first crystalline particles. Then the sample crystallized slowly, as indicated by the gentle slope of the "*S*" curve (Figure 8a). In contrast, the addition of the commercial mordenite zeolite seed decreased substantially the induction period in the case of MOR-2S. The XRD peaks characteristic for MOR phase occurs already after only 1 h of hydrothermal treatment. In addition, the relative crystallinity of the samples increased much faster compared with MOR-2. A fully crystalline sample was obtained already after 8 h of hydrothermal synthesis. Interestingly, the onset of the crystalline particles in this MOR-2S sample is even earlier than that of MOR-2SF, noting that in the latter case the same amount of NH_4F-tailored mordenite zeolite was used as seeds

https://doi.org/10.1021/acs.cgd.3c00427
Cryst. Growth Des. 2023, 23, 6450−6460

to boost the crystallization. Once the short induction period had passed, however, the MOR-2SF sample crystallized as fast as MOR-2S.

In order to understand better the different nucleation behaviors in the early stage of crystallization, the pH of the samples taken out during synthesis was measured (Figure 8b). The pH of the initial aluminosilicate gels prepared at room temperature is the same for MOR-2, MOR-2S and MOR-2SF. In this moment, the presence of seed crystals in the gel does not affect the pH of the system. The hydrothermal treatment of the gel in the oven for 1 h decreased sharply the pH of the synthetic medium, but to different a level depending on the specific synthesis system. In the case of MOR-2, the pH decreased from 13.75 to 12.47 as a result of the hydrolysis and/or condensation of the primary gels.[54] In the case of MOR-2S and MOR-2SF, the pH decreased from 13.75 further to 12.06 and 12.00, respectively. Apparently, the seeds added into the amorphous precursors consumed a certain amount of OH^-, pointing to the dissolution of zeolite seeds added to the synthetic mixture. Following this line, we can reason that the more soluble the seeds are, the higher the amount of consumed OH^-. This is in accordance with the fact that the MOR-F seed with a high Si/Al ratio, high mesopore volume and small crystal size has a higher tendency to dissolve in an alkaline medium than the parent counterpart. Compared with the medium for the synthesis of MOR-2S, the higher solubility of MOR-F should be responsible for the delayed nucleation during the synthesis of MOR-2SF (Figures S5−S6). On the other hand, the small particle size of the synthesized product in the latter case shows clearly that, at least in the present case, the dissolution of zeolite seeds is favorable for the synthesis of zeolites with nanosized dimensions.

3.2.5. Application of the Tailoring Strategy in the Synthesis of Other Zeolites: Tailor-Made Nano-ZSM-5 Seeds for the Synthesis of ZSM-5 Nanosheets. With the aim to test the general applicability of the chemical cutting strategy for nanozeolite synthesis, a nano-ZSM-5 zeolite was prepared through NH_4F etching of MFI-90. This is a crystalline nanosized commercial ZSM-5 zeolite with an aggregated morphology (Figure 9a). After the NH_4F treatment, a substantial decrease of the particle size distribution is achieved, thanks to the segmentation along the interfaces between the crystals building the aggregates[37] (Figure 9b). The tailor-made zeolite was used as seeds for the synthesis of ZSM-5 zeolite (ZSM-5−2, Experimental part). For reference, the parent MFI-90 sample was also used as a seed directly for the synthesis of the second-generation zeolite product (ZSM-5-1).

The XRD patterns of the two obtained zeolite samples are shown in Figure 10. Both samples are high crystalline ZSM-5 zeolites as revealed by the intense peak intensity characteristic of MFI topology. The size and morphology of these two samples were checked by using SEM (Figure 9c, d). While both samples show an elongated morphology along the *c*-axis, which is typical for the synthesis carried out in fluoride medium, these two zeolites differ obviously in the *b*-axis thickness. Specifically, the thickness of the ZSM-5−1 sample varies broadly from 50 to 350 nm along the *b*-axis direction. In contrast, the ZSM-5-2 sample has a more centralized and thinner thickness along the *b*-axis. The synthesis of ZSM-5 nanosheet is a hot topic in recent research.[55−62] In the present work, the successful preparation of nanosheet ZSM-5 zeolite in fluoride medium in the presence of NH_4F treated seeds shows clearly the versatility of the chemical cutting strategy for

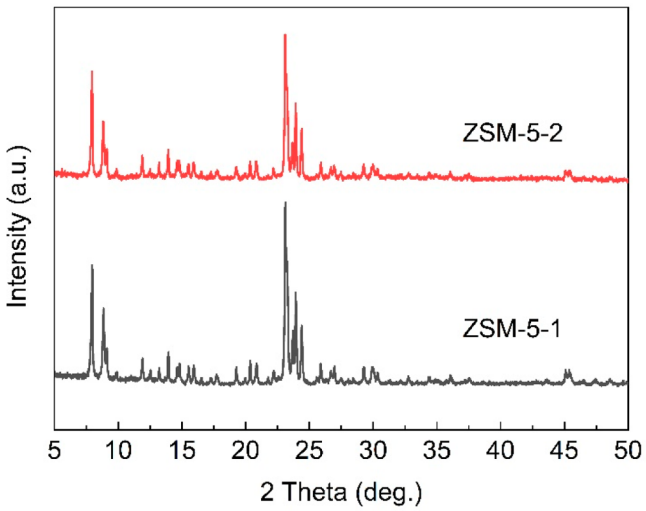

Figure 10. XRD patterns of the ZSM-5 samples.

nanozeolite synthesis. Considering that the synthesis was carried out at 150 °C with a medium NH_4F content, we believe that an optimization of the synthetic parameters can decrease further the length and thickness of the sheet-like crystals.[52,56]

3.2.6. Advantage of the Tailor-Made Seeds for Zeolite Synthesis. One advantage of the present approach is the controllability in tailoring the size of the seed crystals. This is because the seeds are prepared by permanent removal of framework Si and Al atoms. Especially for those zeolites with medium or small pores, or large-pore zeolites with only a one-dimensional channel system, such as MFI, MOR, TON, the dissolution of these zeolite frameworks follows a reversed layer-by-layer mechanism.[24,38] In this case, the particle size of the dissolved products can be controlled conveniently through the tuning of etching time, etchant concentration, etc.[38,40] Also, for this reason, we believe this protocol can be broadly applied to many systems for the preparation of the initial seeds for the synthesis of nanosized zeolites, as this method has the capacity to turn large zeolite crystals into nanosized grains with preserved crystallinity, provided that the type of zeolites can be dissolved following the reversed layer-by-layer manner. In the present work, this is confirmed by the disassembly of both mordenite and ZSM-5 of an aggregative nature (Figures 3a and 9a).

An additional advantage of the present approach is the versatility in tuning the Si/Al ratio of the tailored seeds. This can be achieved through the judicious selection of the parent zeolite, as NH_4F etching has the unique characteristic to remove unbiasedly Si and Al from zeolite framework.[37,40] Hence the particle size of the zeolite crystals can be reduced without altering the initial Si/Al ratio of the selected parent sample. The Si/Al ratio of seeds can be tuned also through the combination of different chemical etchings, as exemplified by the sequential oxalic acid leaching and NH_4F etching in the present work. The use of zeolite seeds with different Si/Al ratios will have a direct impact on the Si/Al ratio of the synthesized products (Table 2). This is achieved through either the change of the pH of the synthesis medium (Figure 8b), or the epitaxial growth that incorporates the zeolite seed directly in the core part of zeolite products.

https://doi.org/10.1021/acs.cgd.3c00427
Cryst. Growth Des. 2023, 23, 6450−6460

4. CONCLUSION

In the present work, NH_4F etching was explored as a "chemical scissors" for the cutting of existing zeolites into nanosized crystals with uniform particle size distribution. The tailor-made nanozeolites are excellent seeds for the synthesis of zeolite products with nanosized dimensions. This was exemplified by the seeded synthesis of mordenite and ZSM-5 zeolites using OH^- and F^- as mineralizers, respectively. The dissolution of the added seeds, at least in the OH^- mediated synthesis medium, is beneficial for the synthesis of zeolites with reduced particle size. This highlights the potential of the solubility of zeolite crystals as an effective element for tuning zeolite nucleation and crystallization. Considering the general applicability of NH_4F etching in the postsynthesis engineering of zeolite particle size, it is believed that this chemical cutting strategy can be applied in many systems aiming for nanosized zeolite synthesis.

■ ASSOCIATED CONTENT

Supporting Information

The Supporting Information is available free of charge at https://pubs.acs.org/doi/10.1021/acs.cgd.3c00427.

Statistical particle size distribution of the seed zeolites (Figure S1), the N_2 adsorption−desorption isotherms and pore size distribution of the mordenite zeolite samples (Figure S2), the statistical particle size distribution of the synthesized mordenite zeolite samples (Figure S3), and the XRD patterns of samples from 0 to 24 h (Figures S4−S6) (PDF)

■ AUTHOR INFORMATION

Corresponding Authors

Shutao Xu − *National Engineering Research Center of Lower-Carbon Catalysis Technology, Dalian Institute of Chemical Physics, Chinese Academy of Sciences, Dalian, Liaoning 116023, China;* orcid.org/0000-0003-4722-8371; Email: xushutao@dicp.ac.cn

Zhengxing Qin − *State Key Laboratory of Heavy Oil Processing, College of Chemistry and Chemical Engineering, China University of Petroleum (East China), Qingdao 266580, China;* orcid.org/0000-0002-0277-9885; Email: zhengxing.qin@upc.edu.cn

Authors

Zihao Wang − *State Key Laboratory of Heavy Oil Processing, College of Chemistry and Chemical Engineering, China University of Petroleum (East China), Qingdao 266580, China; National Engineering Research Center of Lower-Carbon Catalysis Technology, Dalian Institute of Chemical Physics, Chinese Academy of Sciences, Dalian, Liaoning 116023, China*

Tongtong Meng − *State Key Laboratory of Heavy Oil Processing, College of Chemistry and Chemical Engineering, China University of Petroleum (East China), Qingdao 266580, China*

Jiani Xu − *State Key Laboratory of Heavy Oil Processing, College of Chemistry and Chemical Engineering, China University of Petroleum (East China), Qingdao 266580, China; National Engineering Research Center of Lower-Carbon Catalysis Technology, Dalian Institute of Chemical Physics, Chinese Academy of Sciences, Dalian, Liaoning 116023, China*

Yanfeng Shen − *State Key Laboratory of Heavy Oil Processing, College of Chemistry and Chemical Engineering, China University of Petroleum (East China), Qingdao 266580, China*

Yida Zhou − *National Engineering Research Center of Lower-Carbon Catalysis Technology, Dalian Institute of Chemical Physics, Chinese Academy of Sciences, Dalian, Liaoning 116023, China*

Yuhan Liu − *State Key Laboratory of Heavy Oil Processing, College of Chemistry and Chemical Engineering, China University of Petroleum (East China), Qingdao 266580, China; National Engineering Research Center of Lower-Carbon Catalysis Technology, Dalian Institute of Chemical Physics, Chinese Academy of Sciences, Dalian, Liaoning 116023, China*

Dong Fan − *National Engineering Research Center of Lower-Carbon Catalysis Technology, Dalian Institute of Chemical Physics, Chinese Academy of Sciences, Dalian, Liaoning 116023, China*

Xinmei Liu − *State Key Laboratory of Heavy Oil Processing, College of Chemistry and Chemical Engineering, China University of Petroleum (East China), Qingdao 266580, China;* orcid.org/0000-0001-8306-9545

Complete contact information is available at: https://pubs.acs.org/10.1021/acs.cgd.3c00427

Notes

The authors declare no competing financial interest.

■ ACKNOWLEDGMENTS

We appreciate the National Natural Science Foundation of China (NSFC 22178389, 22241801, 22022202, 21972142, 21991092, 21991091, 21991090, 22288101, 22272173), Dalian Outstanding Young Scientist Foundation (2021RJ01). The authors declare no competing financial interest.

■ REFERENCES

(1) Weckhuysen, B.; Yu, J. Recent advances in zeolite chemistry and catalysis. *Chem. Soc. Rev.* **2015**, *44* (20), 7022−7024.

(2) Li, Y.; Yu, J. Emerging applications of zeolites in catalysis, separation and host−guest assembly. *Nature Reviews Materials* **2021**, *6* (12), 1156−1174.

(3) Mintova, S.; Jaber, M.; Valtchev, V. Nanosized microporous crystals: emerging applications. *Chem. Soc. Rev.* **2015**, *44* (20), 7207−7233.

(4) Medeiros-Costa, I.; Dib, E.; Nesterenko, N.; Dath, J.; Gilson, J.; Mintova, S. Silanol defect engineering and healing in zeolites: opportunities to fine-tune their properties and performances. *Chem. Soc. Rev.* **2021**, *50* (19), 11156−11179.

(5) Olsbye, U.; Svelle, S.; Bjorgen, M.; Beato, P.; Janssens, T.; Joensen, F.; Bordiga, S.; Lillerud, K. Conversion of Methanol to Hydrocarbons: How Zeolite Cavity and Pore Size Controls Product Selectivity. *Angew. Chem. Int. Edit* **2012**, *51* (24), 5810−5831.

(6) Al-Khattaf, S.; Ali, S.; Aitani, A.; Zilkova, N.; Kubicka, D.; Cejka, J. Recent Advances in Reactions of Alkylbenzenes Over Novel Zeolites: The Effects of Zeolite Structure and Morphology. *Catal. Rev.* **2014**, *56* (4), 333−402.

(7) Peng, P.; Gao, X.; Yan, Z.; Mintova, S. Diffusion and catalyst efficiency in hierarchical zeolite catalysts. *National Science Review* **2020**, *7* (11), 1726−1742.

(8) Pérez-Ramírez, J.; Christensen, C.; Egeblad, K.; Christensen, C.; Groen, J. Hierarchical zeolites: enhanced utilisation of microporous crystals in catalysis by advances in materials design. *Chem. Soc. Rev.* **2008**, *37* (11), 2530−2542.

(9) Kalvachev, Y.; Todorova, T.; Popov, C. Recent Progress in synthesis and application of nanosized and hierarchical mordenite—A Short Review. *Catalysts* **2021**, *11* (3), 308.
(10) Schmidt, I.; Madsen, C.; Jacobsen, C. Confined space synthesis. A novel route to nanosized zeolites. *Inorganic chemistry* **2000**, *39* (11), 2279−2283.
(11) Tosheva, L.; Valtchev, V. Nanozeolites: synthesis, crystallization mechanism, and applications. *Chemistry of materials* **2005**, *17* (10), 2494−2513.
(12) Ng, E.; Chateigner, D.; Bein, T.; Valtchev, V.; Mintova, S. Capturing ultrasmall EMT zeolite from template-free systems. *Science* **2012**, *335* (6064), 70−73.
(13) Valtchev, V.; Tosheva, L. Porous nanosized particles: preparation, properties, and applications. *Chem. Rev.* **2013**, *113* (8), 6734−6760.
(14) Awala, H.; Gilson, J.; Retoux, R.; Boullay, P.; Goupil, J.; Valtchev, V.; Mintova, S. Template-free nanosized faujasite-type zeolites. *Nature materials* **2015**, *14* (4), 447−451.
(15) Dai, H.; Shen, Y.; Yang, T.; Lee, C.; Fu, D.; Agarwal, A.; Le, T.; Tsapatsis, M.; Palmer, J.; Weckhuysen, B.; et al. Finned zeolite catalysts. *Nat. Mater.* **2020**, *19* (10), 1074−1080.
(16) Choi, M.; Na, K.; Kim, J.; Sakamoto, Y.; Terasaki, O.; Ryoo, R. Stable single-unit-cell nanosheets of zeolite MFI as active and long-lived catalysts. *Nature* **2009**, *461* (7261), 246−249.
(17) Zhang, X.; Liu, D.; Xu, D.; Asahina, S.; Cychosz, K. A.; Agrawal, K. V.; Al Wahedi, Y.; Bhan, A.; Al Hashimi, S.; Terasaki, O.; et al. Synthesis of self-pillared zeolite nanosheets by repetitive branching. *science* **2012**, *336* (6089), 1684−1687.
(18) Na, K.; Jo, C.; Kim, J.; Cho, K.; Jung, J.; Seo, Y.; Messinger, R.; Chmelka, B.; Ryoo, R. Directing zeolite structures into hierarchically nanoporous architectures. *Science* **2011**, *333* (6040), 328−332.
(19) Xu, L.; Ji, X.; Li, S.; Zhou, Z.; Du, X.; Sun, J.; Deng, F.; Che, S.; Wu, P. Self-assembly of cetyltrimethylammonium bromide and lamellar zeolite precursor for the preparation of hierarchical MWW zeolite. *Chem. Mater.* **2016**, *28* (12), 4512−4521.
(20) Roth, W.; Nachtigall, P.; Morris, R.; Wheatley, P.; Seymour, V.; Ashbrook, S.; Chlubná, P.; Grajciar, L.; Položij, M.; Zukal, A.; et al. A family of zeolites with controlled pore size prepared using a top-down method. *Nature Chem.* **2013**, *5* (7), 628−633.
(21) Morris, S.; Bignami, G.; Tian, Y.; Navarro, M.; Firth, D.; Čejka, J.; Wheatley, P.; Dawson, D.; Slawinski, W.; Wragg, D.; et al. In situ solid-state NMR and XRD studies of the ADOR process and the unusual structure of zeolite IPC-6. *Nat. Chem.* **2017**, *9* (10), 1012−1018.
(22) Bai, R.; Song, Y.; Li, Y.; Yu, J. Creating hierarchical pores in zeolite catalysts. *Trends in Chemistry* **2019**, *1* (6), 601−611.
(23) Chen, L.; Sun, M.; Wang, Z.; Yang, W.; Xie, Z.; Su, B. Hierarchically structured zeolites: from design to application. *Chem. Rev.* **2020**, *120* (20), 11194−11294.
(24) Qin, Z.; Pinard, L.; Benghalem, M.; Daou, T.; Melinte, G.; Ersen, O.; Asahina, S.; Gilson, J.; Valtchev, V. Preparation of Single-Crystal "House-of-Cards"-like ZSM-5 and Their Performance in Ethanol-to-Hydrocarbon Conversion. *Chem. Mater.* **2019**, *31* (13), 4639−4648.
(25) Groen, J.; Moulijn, J.; Pérez-Ramírez, J. *Desilication: on the controlled generation of mesoporosity in MFI zeolites* **2006**, *16* (22), 2121−2131.
(26) Jain, R.; Rimer, J. D. Seed-Assisted zeolite synthesis: The impact of seeding conditions and interzeolite transformations on crystal structure and morphology. *Microporous Mesoporous Mater.* **2020**, *300*, No. 110174.
(27) Jain, R.; Mallette, A.; Rimer, J. Controlling nucleation pathways in zeolite crystallization: seeding conceptual methodologies for advanced materials design. *J. Am. Chem. Soc.* **2021**, *143* (51), 21446−21460.
(28) Iyoki, K.; Itabashi, K.; Okubo, T. Progress in seed-assisted synthesis of zeolites without using organic structure-directing agents. *Microporous Mesoporous Mater.* **2014**, *189*, 22−30.
(29) Majano, G.; Darwiche, A.; Mintova, S.; Valtchev, V. Seed-induced crystallization of nanosized Na-ZSM-5 crystals. *Industrial engineering chemistry research* **2009**, *48* (15), 7084−7091.
(30) Yokoi, T.; Mochizuki, H.; Namba, S.; Kondo, J.; Tatsumi, T. Control of the Al Distribution in the Framework of ZSM-5 Zeolite and Its Evaluation by Solid-State NMR Technique and Catalytic Properties. *J. Phys. Chem. C* **2015**, *119* (27), 15303−15315.
(31) Javdani, A.; Ahmadpour, J.; Yaripour, F. Nano-sized ZSM-5 zeolite synthesized via seeding technique for methanol conversions: A review. *Microporous Mesoporous Mater.* **2019**, *284*, 443−458.
(32) Xie, B.; Zhang, H.; Yang, C.; Liu, S.; Ren, L.; Zhang, L.; Meng, X.; Yilmaz, B.; Müller, U.; Xiao, F. Seed-directed synthesis of zeolites with enhanced performance in the absence of organic templates. *Chem. Commun.* **2011**, *47* (13), 3945−3947.
(33) Jon, H.; Ikawa, N.; Oumi, Y.; Sano, T. An insight into the process involved in hydrothermal conversion of FAU to* BEA zeolite. *Chem. Mater.* **2008**, *20* (12), 4135−4141.
(34) Itabashi, K.; Kamimura, Y.; Iyoki, K.; Shimojima, A.; Okubo, T. A working hypothesis for broadening framework types of zeolites in seed-assisted synthesis without organic structure-directing agent. *J. Am. Chem. Soc.* **2012**, *134* (28), 11542−11549.
(35) Cao, K.; Fan, D.; Li, L.; Fan, B.; Wang, L.; Zhu, D.; Wang, Q.; Tian, P.; Liu, Z. Insights into the pyridine-modified MOR zeolite catalysts for DME carbonylation. *ACS Catal.* **2020**, *10* (5), 3372−3380.
(36) Chen, W.; Tarach, K.; Yi, X.; Liu, Z.; Tang, X.; Góra-Marek, K.; Zheng, A. Charge-separation driven mechanism via acylium ion intermediate migration during catalytic carbonylation in mordenite zeolite. *Nat. Commun.* **2022**, *13* (1), 7106.
(37) Qin, Z.; Hafiz, L.; Shen, Y.; Van Daele, S.; Boullay, P.; Ruaux, V.; Mintova, S.; Gilson, J.; Valtchev, V. Defect-engineered zeolite porosity and accessibility. *J. Mater. Chem. A* **2020**, *8* (7), 3621−3631.
(38) Qin, Z.; You, Z.; Bozhilov, K.; Kolev, S.; Yang, W.; Shen, Y.; Jin, X.; Gilson, J.; Mintova, S.; Vayssilov, G.; Valtchev, V. Dissolution Behavior and Varied Mesoporosity of Zeolites by NH_4F Etching. *Chem.—Eur. J.* **2022**, *28* (16), No. e202104339.
(39) Thommes, M.; Kaneko, K.; Neimark, A. V.; Olivier, J. P.; Rodriguez-Reinoso, F.; Rouquerol, J.; Sing, K. S. Physisorption of gases, with special reference to the evaluation of surface area and pore size distribution (IUPAC Technical Report). *Pure and applied chemistry* **2015**, *87* (9−10), 1051−1069.
(40) Qin, Z.; Melinte, G.; Gilson, J.; Jaber, M.; Bozhilov, K.; Boullay, P.; Mintova, S.; Ersen, O.; Valtchev, V. The Mosaic Structure of Zeolite Crystals. *Angew. Chem., Int. Ed. Engl.* **2016**, *55* (48), 15049−15052.
(41) Li, X.; Prins, R.; Van Bokhoven, J. Synthesis and characterization of mesoporous mordenite. *J. Catal.* **2009**, *262* (2), 257−265.
(42) Van Laak, A.; Sagala, S.; Zečević, J.; Friedrich, H.; De Jongh, P.; De Jong, K. Mesoporous mordenites obtained by sequential acid and alkaline treatments−Catalysts for cumene production with enhanced accessibility. *J. Catal.* **2010**, *276* (1), 170−180.
(43) Zhang, J.; Ding, X.; Liu, H.; Fan, D.; Xu, S.; Wei, Y.; Liu, Z. Study on the Framework Aluminum Distributions of HMOR Zeolite and Identification of Active Sites for Dimethyl Ether Carbonylation Reaction. *Acta Chimica Sinica* **2022**, *80* (5), 590−600.
(44) Zhang, L.; Xie, S.; Xin, W.; Li, X.; Liu, S.; Xu, L. Crystallization and morphology of mordenite zeolite influenced by various parameters in organic-free synthesis. *Mater. Res. Bull.* **2011**, *46* (6), 894−900.
(45) Yao, J.; Feng, X.; Fan, J.; He, Y.; Kosol, R.; Zeng, Y.; Liu, G.; Ma, Q.; Yang, G.; Tsubaki, N. Effects of mordenite zeolite catalyst synthesis conditions on dimethyl ether carbonylation. *Microporous Mesoporous Mater.* **2020**, *306*, No. 110431.
(46) Xue, H.; Huang, X.; Ditzel, E.; Zhan, E.; Ma, M.; Shen, W. Coking on micrometer-and nanometer-sized mordenite during dimethyl ether carbonylation to methyl acetate. *Chinese Journal of Catalysis* **2013**, *34* (8), 1496−1503.

https://doi.org/10.1021/acs.cgd.3c00427
Cryst. Growth Des. 2023, 23, 6450−6460

(47) Wen, F.; Ding, X.; Fang, X.; Liu, H.; Zhu, W. Crystal size sensitivity of HMOR zeolite in dimethyl ether carbonylation. *Catal. Commun.* **2021**, *154*, No. 106309.
(48) Ma, M.; Huang, X.; Zhan, E.; Zhou, Y.; Xue, H.; Shen, W. Synthesis of mordenite nanosheets with shortened channel lengths and enhanced catalytic activity. *J. Mater. Chem. A* **2017**, *5* (19), 8887−8891.
(49) Liu, Y.; Zhao, N.; Xian, H.; Cheng, Q.; Tan, Y.; Tsubaki, N.; Li, X. Facilely synthesized H-mordenite nanosheet assembly for carbonylation of dimethyl ether. *ACS Appl. Mater. Interfaces* **2015**, *7* (16), 8398−8403.
(50) Bhan, A.; Allian, A.; Sunley, G.; Law, D.; Iglesia, E. Specificity of sites within eight-membered ring zeolite channels for carbonylation of methyls to acetyls. *J. Am. Chem. Soc.* **2007**, *129* (16), 4919−4924.
(51) Li, B.; Xu, J.; Han, B.; Wang, X.; Qi, G.; Zhang, Z.; Wang, C.; Deng, F. Insight into Dimethyl Ether Carbonylation Reaction over Mordenite Zeolite from in-Situ Solid-State NMR Spectroscopy. *J. Phys. Chem. C* **2013**, *117* (11), 5840−5847.
(52) Qin, Z.; Lakiss, L.; Tosheva, L.; Gilson, J. P.; Vicente, A.; Fernandez, C.; Valtchev, V. Comparative study of nano-ZSM-5 catalysts synthesized in OH− and F− media. *Adv. Funct. Mater.* **2014**, *24* (2), 257−264.
(53) Mintova, S.; Olson, N.; Valtchev, V.; Bein, T. Mechanism of zeolite A nanocrystal growth from colloids at room temperature. *Science* **1999**, *283* (5404), 958−960.
(54) Cundy, C.; Cox, P. The hydrothermal synthesis of zeolites: Precursors, intermediates and reaction mechanism. *Microporous Mesoporous Mater.* **2005**, *82* (1−2), 1−78.
(55) Jeon, M.; Kim, D.; Kumar, P.; Lee, P.; Rangnekar, N.; Bai, P.; Shete, M.; Elyassi, B.; Lee, H.; Narasimharao, K.; et al. Ultra-selective high-flux membranes from directly synthesized zeolite nanosheets. *Nature* **2017**, *543* (7647), 690−694.
(56) Dai, W.; Kouvatas, C.; Tai, W.; Wu, G.; Guan, N.; Li, L.; Valtchev, V. Platelike MFI crystals with controlled crystal faces aspect ratio. *J. Am. Chem. Soc.* **2021**, *143* (4), 1993−2004.
(57) Lv, X.; Yang, M.; Song, S.; Xia, M.; Li, J.; Wei, Y.; Xu, C.; Song, W.; Liu, J. Boosting Propane Dehydrogenation by the Regioselective Distribution of Subnanometric CoO Clusters in MFI Zeolite Nanosheets. *ACS Appl. Mater. Interfaces* **2023**, *15*, 14250.
(58) Wang, C.; Fang, W.; Liu, Z.; Wang, L.; Liao, Z.; Yang, Y.; Li, H.; Liu, L.; Zhou, H.; Qin, X.; et al. Fischer−Tropsch synthesis to olefins boosted by MFI zeolite nanosheets. *Nat. Nanotechnol.* **2022**, *17* (7), 714−720.
(59) Zhang, J.; Ren, L.; Zhou, A.; Li, W.; Shang, S.; Liu, Y.; Jia, Z.; Liu, W.; Zhang, A.; Guo, X.; Song, C. Tailored synthesis of ZSM-5 nanosheets with controllable b-axis thickness and aspect ratio: Strategy and growth mechanism. *Chem. Mater.* **2022**, *34* (7), 3217−3226.
(60) Wang, X.; Ma, Y.; Wu, Q.; Wen, Y.; Xiao, F. Zeolite nanosheets for catalysis. *Chem. Soc. Rev.* **2022**, *51*, 2431.
(61) Zhang, J.; Zhou, A.; Gawande, K.; Li, G.; Shang, S.; Dai, C.; Fan, W.; Han, Y.; Song, C.; Ren, L.; et al. b-Axis-Oriented ZSM-5 Nanosheets for Efficient Alkylation of Benzene with Methanol: Synergy of Acid Sites and Diffusion. *ACS Catal.* **2023**, *13*, 3794−3805.
(62) Zhang, L.; Song, Y.; Li, G.; Zhang, Q.; Zhang, S.; Xu, J.; Deng, F.; Gong, Y. F-assisted synthesis of a hierarchical ZSM-5 zeolite for methanol to propylene reaction: ab-oriented thinner dimensional morphology. *RSC Adv.* **2015**, *5* (75), 61354−61363.

https://doi.org/10.1021/acs.cgd.3c00427
Cryst. Growth Des. 2023, 23, 6450−6460